UCRL-11619 Rev. 1

University of California

Ernest O. Lawrence Radiation Laboratory

NUMERICAL MODEL OF AN ION-CYCLOTRON WAVE EXPERIMENT

TWO-WEEK LOAN COPY

This is a Library Circulating Copy which may be borrowed for two weeks. For a personal retention copy, call Tech. Info. Division, Ext. 5545

Berkeley, California

DISCLAIMER

This document was prepared as an account of work sponsored by the United States Government. While this document is believed to contain correct information, neither the United States Government nor any agency thereof, nor the Regents of the University of California, nor any of their employees, makes any warranty, express or implied, or assumes any legal responsibility for the accuracy, completeness, or usefulness of any information, apparatus, product, or process disclosed, or represents that its use would not infringe privately owned rights. Reference herein to any specific commercial product, process, or service by its trade name, trademark, manufacturer, or otherwise, does not necessarily constitute or imply its endorsement, recommendation, or favoring by the United States Government or any agency thereof, or the Regents of the University of California. The views and opinions of authors expressed herein do not necessarily state or reflect those of the United States Government or any agency thereof or the Regents of the University of California.

Submitted to Physics of Fluids

UCRL-11619 Rev. 1

UNIVERSITY OF CALIFORNIA

Lawrence Radiation Laboratory
Berkeley, California

AEC Contract No. W-7405-eng-48

NUMERICAL MODEL OF AN ION-CYCLOTRON WAVE EXPERIMENT

Gordon W. Hamilton

January 6, 1965

NUMERICAL MODEL OF AN ION-CYCLOTRON WAVE EXPERIMENT*

Gordon W. Hamilton†

Lawrence Radiation Laboratory
University of California
Berkeley, California

January 6, 1965

ABSTRACT

A numerical model has been constructed to demonstrate the propagation and absorption of ion-cyclotron waves in a previously reported experiment. Ion-cyclotron waves in a deuterium plasma induced by a radially applied 8.3-Mc electric field propagate in a magnetic-mirror field to a resonance region where the ion-cyclotron frequency approaches the wave frequency. The numerical model considers the wave propagation in the nonuniform divergenceless magnetic field with spatially nonuniform plasma parameters, subject to boundary conditions modeled after the experiment. The model is based on the macroscopic equation of motion, the generalized Ohm's law, the wave equation, an equivalent resistivity representing the effect of ion-cyclotron damping, and damping by collisions between deuterons and other particle species. The equations are solved numerically by a single-line block over-relaxation technique. The numerical results are compared with the experimental wave measurements and also provide information regarding current distributions, wave polarizations, evanescent compressional waves, and reflections from the resonance under certain conditions.

I. INTRODUCTION

A. Statement of Problem

A review of experiment on ion-cyclotron resonance in plasmas, has been published by Hooke and Rothman.[1] In most of these experiments the ion-cyclotron waves are excited by an induction coil (around the outside of the plasma chamber) that applies an rf magnetic field in the radial and axial directions of a cylindrical geometry. In our experiment the wave was excited by the direct application of a radial rf electric field to the plasma.[2] A further difference is in the significantly steeper magnetic-field gradient employed in our experiment for the transition between the excitation region and the ion-cyclotron resonance.

A large literature exists on the theory of plasma waves and ion-cyclotron damping. Most pertinent to this paper are the works of Stix;[3] Allis, Buchsbaum, and Bers;[4] and DeSilva;[5] each of these contains a large bibliography on these topics. More recent theoretical studies of ion-cyclotron damping have been on aspects such as the effects of collision,[6,7] an approximation by the method of geometrical optics,[8] and several studies of charge-particle motion near cyclotron resonances.[9,10,11]

In general the various theories are concerned with certain complications separately but do not attempt to consider all the interrelationships between the effects. In order to clarify certain aspects of this experiment a theoretical model is required for the propagation and absorption of ion-cyclotron waves in a bounded plasma in a nonuniform divergenceless magnetic field with provisions for collisions between species, propagation in various directions relative to the external magnetic field, and non-uniformities in temperatures and densities of ion, electrons, neutral

particles, and impurity ions. Such a model has been constructed numerically to solve the magnetohydrodynamic equations and thereby determine the nature of the propagation and absorption of ion-cyclotron waves in arbitrarily assumed nonuniform conditions.

The numerical model is based on an impedance tensor derived from the macroscopic equation of motion and the generalized Ohm's law. Since these equations do not include the cyclotron damping mechanism, an equivalent resistivity tensor is derived and added to the impedance tensor to represent the effect of ion-cyclotron damping. The resulting tensor equation is combined with a wave equation and solved numerically. The solution is determined by a set of physically realistic boundary conditions.

B. Notation

Vectors, unit vectors, tensors, and matrices are indicated as in these examples: vector, $\underline{E}$; unit vector, $\hat{r}$; tensor or matrix, $\underline{\underline{z}}$. Vector and tensor products are always dot products unless the cross product is specified. The dot is usually omitted.

Time-dependent quantities associated with the wave are actually real functions of position and time, but are replaced by the real part of their complex Fourier transforms. When monochromatic time dependence is assumed,

$$\underline{E}(\underline{r}, t) = \mathrm{Re}[\,\underline{E}(\underline{r})\, e^{-i\omega t}].$$

In keeping with common practice, we freely replace the real vector $\underline{E}(\underline{r}, t)$ with the complex vector $\underline{E}(\underline{r})$, which consists of three complex components

each with an amplitude and a phase angle. The factor $e^{-i\omega t}$ and the notation Re are dropped since they occur in every term of the equations.

Superscripts denote the components of vectors. The four species-ions, electrons, neutral atoms, and heavy impurity ions-are indicated by the subscripts i, e, n, and I. When the species is not indicated it is assumed to be ions.

Since a nonuniform magnetic field is not everywhere parallel to the axis of symmetry, the terms "transverse" and "longitudinal" refer to the directions perpendicular and parallel to the external magnetic field. The term "axial" indicates the direction parallel to the axis of symmetry.

The symbols used in this paper are listed below alphabetically:

$\underline{b}$ wave magnetic field

$\underline{B}$ externally applied magnetic field

c velocity of light

e electron charge

$\underline{E}$ wave electric-field vector

$f(u^{z'})$ distribution function for longitudinal ion velocities

$\underline{j}$ wave current density

k wave number

m particle mass

n particle density

$\underline{P}_{ij}$ rate of momentum transfer per unit volume from species j to species i

$\underline{P} = \nabla\times(\nabla\times\underline{E})$ defined by (2.15)

P_{cyc} power absorption per unit volume by cyclotron damping

$\underline{\underline{r}}_c$ cyclotron resistivity tensor

t time

$\underline{u}$ velocity of an individual particle

$\underline{v}$ macroscopic velocity of a species

$\underline{\underline{x}}$ quasi-reactive tensor

$\underline{\underline{z}}$ impedance tensor

z_{xx}, z_{xy}, z_{zz} matrix elements of $\underline{\underline{z}}$, defined by (2.14)

β^+ defined by (2.11)

γ momentum-transfer coefficient

μ_o permeability of free space

$\nu_{ni} = n_i \sigma_{ni} \bar{u}$ ion-neutral collision frequency

$\underline{\underline{\eta}}$ ohmic resistivity tensor

$\eta_\perp$ transverse ohmic resistivity

$\eta_\parallel$ longitudinal ohmic resistivity

η_c magnitude of cyclotron resistivity tensor

ρ, θ, ζ nonorthogonal coordinates defined in Sec. II. F. 1

$\rho_i = n_i m_i$ ion-mass density

ρ_1 complex mass density

σ_{ni} charge-transfer cross section

ω wave frequency

$\omega_c = eB/m_i$ ion-cyclotron frequency

$\Omega = \frac{\omega}{\omega_c} \frac{\rho_1}{\rho_i}$ (This parameter approaches unity at the ion-cyclotron resonance).

II. THEORY

A. Magnetohydrodynamic Equations

The set of equations describing the propagation of nonresonant magnetohydrodynamic (MHD) waves in a medium consisting of singly charged ions, electrons, neutral atoms, and heavy impurity ions consists of a macroscopic equation of motion, a generalized Ohm's law, and two linearized Maxwell equations:

$$nm_i \frac{\partial v_i}{\partial t} = \underline{j} \times \underline{B} + \underline{P}_{in} + \underline{P}_{iI}, \tag{2.1a}$$

$$\underline{E} + \underline{v} \times \underline{B} = \underline{\eta} \cdot \underline{j} + \underline{j} \times \underline{B}/en, \tag{2.2}$$

$$\nabla \times \underline{b} = \mu_o \underline{j}, \tag{2.3}$$

$$\nabla \times \underline{E} = - \frac{\partial \underline{b}}{\partial t}. \tag{2.4}$$

DeSilva[5] has derived this set of equations under the following approximations:

a. Linearity (i.e., $b \ll B$),

b. Charge quasi-neutrality (i.e., $n_i \approx n_e = n$),

c. Neglect of ∇p,

d. Neglect of terms of the order m_e/m_i,

e. Neglect of displacement current; this is valid when the plasma dielectric constant $[K = 1 + (nm_i/\epsilon_o B^2)]$ is much larger than unity,

f. Neglect of $\underline{v} \cdot \nabla \underline{v}$ terms.

The Hall-effect term in (2.2), $\underline{j} \times \underline{B}/en$, is the term through which the effect of the ion-cyclotron resonance enters these equations. This term is often dropped by authors who restrict themselves to Alfvén waves

of frequencies far below the ion-cyclotron resonance. However, we have not yet inserted the ion-cyclotron damping mechanism into these equations.

B. Collisional Damping Mechanisms

Three types of collisional damping mechanisms have been introduced by momentum-transfer terms, each of which is considered proportional to the relative macroscopic velocity of ions with respect to some other species:

$$\underline{P}_{ei} = en\,\underline{\underline{\eta}}\cdot j = e^2n^2\,\underline{\underline{\eta}}\cdot(\underline{v}_i - \underline{v}_e),$$

$$\underline{P}_{ni} = \gamma_n(\underline{v}_i - \underline{v}_n) = \frac{-i\omega\rho_n}{1-i\omega/\nu_{ni}}\,\underline{v}_i\,,$$

$$\underline{P}_{Ii} = \gamma_I(\underline{v}_i - v_I).$$

Transfer of momentum from ions to any other species is a viscosity effect that inhibits the transverse wave motion. Momentum transfer between electrons and other species is qualitatively similar, but is smaller in magnitude by the ratio m_e/m_i and is therefore neglected with the exception of the ion-electron momentum transfer. Since $\underline{P}_{ie} = -\underline{P}_{ei}$, these terms cancel in the equation of motion (2.1a), and generate the ohmic resistivity term $(\underline{\underline{\eta}}\cdot\underline{j})$ in the generalized Ohm's law (2.2). The ohmic resistivity is a tensor of the form

$$\underline{\underline{\eta}} = \begin{pmatrix} \eta_\perp & 0 & 0 \\ 0 & \eta_\perp & 0 \\ 0 & 0 & \eta_\parallel \end{pmatrix},$$

where $\eta_\perp$ and $\eta_\parallel$, the ohmic resistivities across and parallel to the magnetic field, have been computed by Spitzer.[12]

Since the ion velocity perpendicular to the magnetic field can become large at the resonance, the rate of momentum transfer and consequent damping due to all three collision processes becomes large at the resonance. In an ion-cyclotron-heating experiment it is necessary to ascertain which process is primarily responsible for wave damping observed at the resonance.

DeSilva has shown that the effects of $\underline{P}_{ni}$ may be represented by a complex mass density.[5] The complex density can also include the effect of $\underline{P}_{Ii}$. We can therefore rewrite the equation of motion as

$$\rho_1 \frac{\partial \underline{v}_i}{\partial t} = \underline{j} \times \underline{B}, \qquad (2.1b)$$

where the complex mass density ρ_1 includes the effects of neutral atoms and heavy impurity ions

$$\rho_1 = nm_i + \frac{\rho_n}{1-i\omega/\nu_{ni}} + \frac{i\gamma_I}{\omega}. \qquad (2.5)$$

C. Derivation of Impedance Tensor from the MHD Equations

The set of equations (2.1b), (2.2), (2.3), and (2.4) involve four complex-vector unknowns associated with the wave: $\underline{E}$, $\underline{b}$, $\underline{j}$, and $\underline{v}_i$. The four equations can be solved analytically if the parameters ρ_1, $\underline{\eta}$, and $\underline{B}$ are spatially homogeneous and if purely axial propagation is assumed {i.e., with solutions of the form $f(r)\exp[i(pz-\omega t)]$}. In the present experiment these conditions do not pertain, and it is necessary to solve the equations under the more general assumptions that the parameters ρ_1, $\underline{\eta}$, and $\underline{B}$ are arbitrarily specified functions of positon with axial symmetry, and that the propagation will be in unknown directions [i.e., with solutions of the form $f(r,z)\,e^{-i\omega t}$]. These generalizations require numerical techniques for solution.

The set of four equations may be combined into one equation with one unknown. For the numerical technique it is convenient to eliminate all unknowns except $\underline{E}$. This is accomplished first by combining Eqs. (2.1b) and (2.2) to eliminate $\underline{v}_i$, thereby obtaining another form of generalized Ohm's law. We then combine Eqs. (2.3) and (2.4) to eliminate $\underline{b}$ and obtain the wave equation, replacing the time derivative with $-i\omega$. After some algebra to express the first result in tensor form, we have the two equations

$$\underline{E} = \underline{\underline{z}} \cdot \underline{j} \qquad \text{(generalized Ohm's law)} \qquad (2.6)$$

and

$$\nabla \times (\nabla \times \underline{E}) = i\omega\mu_o \underline{j} \qquad \text{(wave equation).} \qquad (2.7)$$

Here the impedance tensor $\underline{\underline{z}}$ is defined by the new generalized Ohm's law (2.6); its inverse $\underline{\underline{z}}^{-1}$ is the conductivity tensor used by some authors.[4,6] It is related to the plasma dielectric tensor by the relation $\underline{\underline{K}} = \underline{\underline{I}} + (i/\omega\epsilon_o)\underline{\underline{z}}^{-1}$.

The impedance tensor is composed of a Hermitian part and an anti-Hermitian part. The Hermitian part includes all the damping mechanisms, whereas the anti-Hermitian part describes the purely reactive impedance.

D. Equivalent Cyclotron Resistivity

Before proceeding to the solution of Eqs. (2.6) and (2.7), we must insert the ion-cyclotron damping mechanism into the impedance tensor. We do this by computing an estimate of the power absorption per unit volume by ion-cyclotron damping following Stix,[3] Sec. 8.2. We then express this power density in a form analogous to $P_{cyc} = r_c j^2$, thus defining a resistivity

tensor $\underline{r}_c$ to introduce the effect of cyclotron damping. In this model we are considering only the resistive effect of phase mixing, ignoring the reactive effect. Stix[3] finds that the reactive correction due to finite ion temperatures may be ignored if $\alpha_{-1}^2 \gg 1$, where $\alpha_{-1} = [\omega - \omega_c / k\,\overline{u^{z'}}]$ and $\overline{u^{z'}}$ is the ion thermal velocity parallel to the magnetic field. Sachs[6] finds an almost identical criterion that justifies the use of moments of the kinetic equations, which is essentially the method used here. We find that for conditions of this experiment this criterion is satisfied except for a region within about 2 cm of the exact resonance. Most of the cyclotron power absorption occurs before the wave propagates into this region.

Following Stix's computation,[3] we find the power absorbed by ion-cyclotron damping per unit volume is

$$P_{cyc} = \frac{n e^2}{4m} \left| E^{x'} + iE^{y'} \right|^2 \beta^+, \tag{2.8}$$

where

$$\beta^+ = \int_{-\infty}^{\infty} du^{z'}\, f(u^{z'}) \left(1 - \frac{ku^{z'}}{\omega}\right) \frac{\sin(\omega - \omega_c - ku^{z'})t}{(\omega - \omega_c - ku^{z'})} .$$

We are using a Cartesian (x' - y' - z') coordinate system such that the z' axis is parallel to the external magnetic field at a given point.

The integral β^+ is a function of the time for which an average ion remains in the conditions described by the equation of motion. In a non-uniform magnetic field this is usually the time required for a resonant ion to move into a significantly different magnetic field due to its axial velocity. It is impractical to determine this time accurately, but the integral can be evaluated when the time is sufficiently short or sufficiently long for the two limiting cases:

a. If $(\omega-\omega_c - ku^{z'})\,t \ll 1$, the sine can be replaced with its argument, and β^+ is linearly proportional to time:

$$\beta^+ \rightarrow \int_{-\infty}^{\infty} du^{z'}\, f(u^{z'})\,(1 - \frac{ku^{z'}}{\omega t}) . \qquad (2.9)$$

In this limit the relative phase angle between the circularly polarized E^+ component and the ion gyro velocity is constant.

b. If $(\omega-\omega_c - ku^{z'})\,t \gg 2\pi$, we can consider that the factor $f(u^{z'})\,(1 - ku^{z'}/\omega t)$ is virtually constant in a velocity interval over which the sine function oscillates several times. The ratio $[\sin(\omega-\omega_c-ku^{z'})t/(\omega-\omega_c-ku^{z'})]$ behaves like a delta function, and the integral approaches the following result for asymptotically long times:

$$\beta^+ \rightarrow \frac{\pi\omega_c}{k\omega}\, f(\frac{\omega-\omega_c}{k}) . \qquad (2.10)$$

For times between these two limits, the integral will oscillate for several cycles. It is out of the question to compute details of the oscillation without knowledge of the time t, so we simply extend the two limiting cases (2.9) and (2.10) until they intersect. The damping power is computed by each of these equations, and we use whichever is smaller, usually (2.10). The propagation constant k is estimated by the phase velocity of the torsional mode

$$k \approx \frac{\omega}{B}\sqrt{\frac{\mu_o \rho_1}{1-\Omega}} .$$

(This estimate can be checked after solution of the equations.)

By use of the generalized Ohm's law (2.6) and the hermiticity of the resistive and reactive tensors, Eq. (2.8) can be put in the following form after some algebra:

$$P_{cyc} = 1/2\ \underline{j}^* \cdot \underset{\sim}{r}_c \cdot \underline{j}\ . \tag{2.11}$$

The cyclotron resistivity tensor is therefore defined as

$$\underset{\sim}{r}_c = \eta_c \begin{pmatrix} 1 & i & 0 \\ -i & 1 & 0 \\ 0 & 0 & 0 \end{pmatrix}, \tag{2.12}$$

where

$$\eta_c = \frac{B^2 \beta^+}{2nm} \left(\frac{\omega_c}{\omega} - 1\right)^2 .$$

Examining this result, we first find that $\underset{\sim}{r}_c$ is Hermitian and that consequently the cyclotron power absorption computed by (2.11) is real. The factor β^+ causes the cyclotron resistivity to be large near the cyclotron resonance and vanishingly small elsewhere. The breadth of the resonant regime is determined by the ion thermal velocity through the distribution function $f(u^{z'})$. The off-diagonal matrix elements have the effect of applying the cyclotron damping only to the rotating component of the transverse wave that is left-circularly polarized; i.e., in the direction of ion gyration. It may appear that the factor $[(\omega_c/\omega) - 1]^2$ introduces the incorrect behavior when $\omega_c \to \omega$ near the resonance, but this is merely due to the definition $P_{cyc} = 1/2\ \underline{j}^* \cdot \underset{\sim}{r}_c \cdot \underline{j}$. The factor $[(\omega_c/\omega) - 1]^2$ is cancelled by the great increase in the transverse current at the resonance. Near the resonance the cyclotron resistivity is one or two orders of magnitude larger than the ohmic resistivity for typical conditions.

E. Total Impedance Tensor

We now add the cyclotron resistivity to the impedance tensor previously derived, thus inserting the mechanism of ion cyclotron damping into the generalized Ohm's law (2.6). The total impedance tensor is now the sum of the ohmic resistivity tensor, the cyclotron resistivity tensor, and the quasi-reactive tensor multiplied by i.

$$\underset{\sim}{z} = \underset{\sim}{\eta} + \underset{\sim}{r}_c + i\,\underset{\sim}{x} = \begin{pmatrix} z_{xx} & z_{xy} & 0 \\ -z_{xy} & z_{xx} & 0 \\ 0 & 0 & z_{zz} \end{pmatrix} \qquad (2.13)$$

where, for abbreviation,

$$z_{xx} = \eta_\perp + \eta_c + iB^2/\omega\rho_1$$
$$z_{xy} = i\,\eta_c + B/en$$
$$z_{zz} = \eta_\parallel .$$

F. Numerical Solution

The numerical techniques are briefly outlined in this section and described in more detail in reference 13.

Having derived the impedance tensor $\underset{\sim}{z}$, which is assumed to be a known function of position in an inhomogeneous plasma, we are ready to commence the numerical solution of the equation formed by combining (2.6) and (2.7):

$$\nabla \times (\nabla \times \underline{E}) = i\omega\mu_o\, \underset{\sim}{z}^{-1} \cdot \underline{E} \equiv \underline{P} . \qquad (2.14)$$

[Here we have defined the vector $\underline{P}$ as an abbreviation for $\nabla \times (\nabla \times \underline{E})$.]

1. Coordinate System

In a cylindrical geometry it is normal to use cylindrical polar coordinates. However, this results in a computational instability driven by the axial component of the wave, since the flux lines are not parallel to the z axis in a magnetic mirror. The instability can be eliminated by choosing a coordinate system such that the transverse wave has no axial component, i.e., such that the transverse coordinate lines are orthogonal to magnetic flux lines. The axial coordinate lines are specified parallel to the z axis to simplify the boundaries. This combination of transverse and axial coordinate lines defines the nonorthogonal curvilinear coordinate system illustrated by Fig. 1. The coordinates are designated as ρ, θ, and ζ, in analogy to the cylindrical polar coordinates r, θ, and z. Equation (2.13) must be transformed to this coordinate system.

2. Mesh System

A mesh system illustrated by Fig. 2 is established in the ρ - ζ plane along coordinate lines, in preparation for conversion of the differential equation (2.14) to difference equations. The mesh should be as fine as possible to improve the accuracy and the computational stability. The limitations are the computer's memory and the time requirement. These requirements impose a limit of about 1400 mesh points, which determines the mesh interval. The mesh system consists of 14 axial mesh lines at intervals (Δr) of 0.762 cm and 99 transverse mesh lines at intervals (Δz) of about 1 cm in the plasma and 0.5 cm in the end insulator.

3. Conversion to Difference Equations

We now convert the differential equation (2.14) to a set of finite difference equations, in which the derivatives involved in $\nabla \times (\nabla \times \underline{E})$ at each mesh point are approximated by the differences in $\underline{E}$ at neighboring points.

At each mesh point we have three complex linear difference equations resulting from the three components of (2.14), and three complex unknowns (E^{ρ}, E^{θ}, and E^{ζ}). The system of about 3300 simultaneous nonsingular complex linear equations is (in principle) solvable. The solution is performed by an iterative method that converges to a solution within the desired accuracy, provided that the matrix representing the system of equations is computationally stable.[14]

III. EXPERIMENTAL APPARATUS AND BOUNDARIES

The plasma is produced from deuterium gas at 5.0×10^{-3} torr pressure and is contained in a copper cylinder 19.8 cm in diameter and 94.0 cm long, as shown in Fig. 3. The external magnetic field is supplied by the coils shown and is normally adjusted to provide a mirror field of approximately 1.9 teslas at the ends and 1.0 tesla in the center. These fields correspond to $\Omega = 0.45$ and $\Omega = 1.1$, where Ω is the parameter that approaches 1.0 at the resonance. The axial and radial magnetic-field intensities are shown by Fig. 4. The copper cylinder is closed by insulating end plates in one of which is mounted a coaxial molybdenum electrode of 6.25-cm diameter and 7.5-cm length. Inside the copper cylinder at the driving end is an outer electrode, the radius of which is designed to intersect the magnetic-field lines that just miss the cylinder walls at the midplane. After plasma preparation, an 8.3-Mc electric field is applied radially for 1.0 msec. Experimental wave measurements have been previously reported.[2]

The boundary conditions used for the numerical solution were closely modeled after the experimental apparatus:

(a) Electrode surfaces were assumed to be in contact with the plasma because of rf currents at these surfaces. The electric-field components parallel to these surfaces are therefore constrained to be zero.

(b) The end screen is intended to be in electrical contact with the plasma and there is evidence that contact is actually established. The electric field parallel to the end screen is also constrained to be zero.

(c) The side wall is evidently insulated from the plasma by a layer of cool gas perhaps a few millimeters thick, according to wave measurements near the side walls. DeSilva has shown in his Appendix F that the condition at the interface between the plasma and the insulating layer is $E^r = E^\theta = E_r^z = 0$, provided the layer thickness falls between certain limits.[5]

(d) The axial center line must have conditions such that the divergences of $\underline{E}$, $\underline{b}$, $\underline{j}$, and $\underline{v}$ are not infinite. This results in the condition $E^r = E^\theta = E_r^z = 0$.

(e) The quartz insulator and its boundaries were believed to have an effect on the wave excitation, and were therefore included in the computer model. The mesh system illustrated by Fig. 2 was extended into the insulator, where the mesh interval Δz was reduced to 0.5 cm because of the steep field gradients in the insulator. The wave equation in the insulator takes the form

$$\nabla \times (\nabla \times \underline{E}) = - (\omega^2/c^2) \, K \underline{E}, \qquad (3.1)$$

where the displacement current is considered but the conduction current is not, and where K is the dielectric constant of the insulator. This wave equation was converted to difference equations and solved with Eq. (3.1) used in place of (2.14) in the insulator.

(f) The boundaries around the insulator were treated appropriately. Tangential components of electric fields are required to be zero at conducting surfaces. An rf potential of 1000 V was specified between the electrodes. The inner electrode is at the same potential as the conducting surface at the outer face of the insulator, and the outer electrode is at the same ground potential as the outer wall. It was required that $\underline{b}$, E^r, E^θ, and the axial component of the displacement be continuous across the interface between the insulator and the plasma.

IV. NUMERICAL RESULTS

A. Presentation of Results

After a solution for $\underline{E}$ at each mesh point was found, the solution was converted into $\underline{b}$ and $\underline{j}$, by (2.4) and (2.7). The solutions were converted to polar form and presented in the form of contour plots produced by a plotter as part of the output. Each contour on Figs. 5 through 8 represents a line of equal phase or of equal amplitudes of $\underline{b}$ or $\underline{j}$. The tabular output must also be consulted in order for one to understand some aspects of these plots.

The contour interval for phase angles is 30°. In the absence of reflections, the wavelength can be determined by measuring the spacing between contours and multiplying by 12. The contour interval for amplitudes is 10% of the maximum amplitude found in the chamber, and is therefore different for each plot, as noted on the figures.

B. Solution of Equations for a Moderately High Density

Figures 5 and 6 show a solution that is fairly easy to understand because of the lack of complications that are discussed in Sec. IV.C. The plasma parameters pertaining to this solution are as follows:

ion density	$1.6 \times 10^{20} m^{-3}$
neutral-particle density	0
impurities	0
ion temperature	50 eV
electron temperature	10 eV
magnetic field	standard mirror field described in Sec. III
location of resonances	z = 46 cm and z = 54 cm.

A complete set of graphical results showing phases and amplitudes of all components of $\underline{E}$, $\underline{b}$, and $\underline{j}$ consists of 18 plots. However, some of this information is redundant, and we shall therefore not reproduce all 18 plots.

1. Wave Currents

Wave rf currents originate at the center electrode following an annular tube of flux defined by the electrode radius. A similar annular current sheet is defined by the inner radius of the outer electrode. Most of the current flows longitudinally to the vicinity of the ion-cyclotron resonance before flowing transversely to complete the circuit between the two current sheets. The two current sheets are most clearly seen on the plot showing the amplitude of j^{ζ}. Integrating over area, we find that the total axial currents at the ends of the two electrodes are equal in magnitude (about 4000 A) but opposite in phase.

The transverse wave current consists of ρ and θ components that are almost equal in magnitude but 90° out of phase. This is because most of the transverse current consists of ions following circular or spiral orbits. The difference between j^{ρ} and j^{θ} is due mostly to the transverse electron current, which is almost entirely in the $\hat{\theta}$ direction and cancels some of the j^{θ} ion current.

The effect of inductance is to minimize the volume enclosed between the annular rf current sheets. This is the reason the current enters and leaves the electrodes at the outer edge of the inner electrode and the inner edge of the outer electrode.

The annular current sheets were experimentally indicated by discontinuities in measurements of b^{θ} and by direct evidence of plasma bombardment at the edges of electrodes.

The transverse wave current becomes large at the resonance because of the large ion orbits and consequent low impedance. All types of wave damping are therefore enhanced at the resonance. By comparing the equivalent cyclotron resistivity with the ohmic resistivity and with the equivalent resistivities due to other species,[13] we can ascertain that ion-cyclotron damping dominates for this set of conditions.

2. Wave Polarization

The relative phase of b^{ρ} and b^{θ} may be deduced either from the tabular output or from the dashed phase contours of Fig. 6 which designate the contours of 0° phase angle. We find a 90° phase difference between the two transverse components of $\underline{E}$, $\underline{b}$, and $\underline{j}$ at all points between the two annular current sheets. The wave is elliptically polarized in the "left" direction (the direction of ion gyration) in this region. The major axis of

the elliptical polarization is in the $\hat{\rho}$ direction for the $\underline{E}$ and $\underline{j}$ wave fields and in the $\hat{\theta}$ direction for the $\underline{b}$ wave field. As the wave approaches resonance, the polarization becomes nearly circular rather than elliptical. This is evident in the amplitude plots showing b^{ρ} and E^{θ} increasing as resonance is approached. All this is characteristic of the torsional mode, also called the T mode or the slow hydromagnetic mode, which is the mode this experiment was designed to excite.

From the contour phase plots of Fig. 6 we can see a large discontinuity in the phase of b^{θ} at the annular current sheets, but no discontinuity in the phase of b^{ρ}. This shows that the relative phase of b^{ρ} and b^{θ} undergoes a large change at the current sheet. The wave is elliptically polarized in the right direction within the magnetic images of the two electrodes, but in left direction in the annulus between the electrodes. (The volumes defined by the flux lines intersecting the electrodes are called magnetic images.)

Next we notice from Fig. 6 that that b^{ζ} is large only within the electrode images. The combination of large b^{ζ} and right elliptical polarization is characteristic of the compressional mode (also called the TLA mode or the fast hydromagnetic mode), which has been studied by Swanson[15] and by Spillman.[16]

Since the compressional mode is cut off for the densities of this experiment, the wave in the electrode images must be evanescent, not propagating. It is excited by the tangential currents (j^{θ}) in the annular current sheets, as a consequence of the finite geometry. The energy in the compressional mode (estimated by integrating $b^2/2\mu_o$ over the volume) is 10% or less than the energy in the torsional mode, for this set of conditions. The compressional mode is an unexpected finding in the numerical model, but is consistent with the experimental measurements of b^{θ}.

3. Wave Amplitudes

The radial variation of the wave amplitude is determined by the boundary conditions and by the annular current sheets. Between the two current sheets the dominant wave components (E^{ρ} and b^{θ}) are proportional to $1/r$.

The wave is strongly damped near the resonance. For this set of conditions the damping mechanism is ion-cyclotron damping, since neutral particles and impurities are assumed to be absent and the electron temperature is high enough that ohmic damping is unimportant. The very small wave transmitted through the resonance is attenuated by two orders of magnitude and is too weak to appear on an amplitude plot of this contour interval, although it shows up on the phase contour plots.

Some very small reflections in the region 10 cm < z < 40 cm can be seen in the amplitude plots for transverse components of b, Fig. 6. (The contour presentation is a very sensitive indicator for standing waves.) The small standing waves with wavelengths of about 9 cm are generated by reflections from the resonance. The wavelength of the ion-cyclotron wave in this region (determined from the spacing between 30° contours) is about 18 cm. This is consistent with the wavelength computed from the analytic theory for the torsional mode.

The small wave that propagates through the resonance is reflected from the conducting end screen, setting up a standing wave pattern in the downstream end of the chamber. In contrast to the standing waves previously discussed, the incident and reflected waves are almost equal in amplitude. Consequently the phase undergoes a discontinuity of almost 180° at the nodes. This standing wave pattern appears on the phase plots as closely grouped

contours at the nodes in the downstream end of the chamber. The irregular contours near the outer wall at the downstream end are caused by the tendency of the wave to follow flux lines in the magnetic mirror field.

As the torsional wave propagates in the nonresonant region between the driving electrodes and the coordinate $z = 40$ cm, we find the amplitudes of the transverse wave change as follows:

b^ρ increasing	b^θ increasing slightly	(Fig. 6)
E^ρ decreasing	E^θ increasing	

(For brevity, we will not reproduce the graphical solutions for $\underline{E}$ in this paper.)

For these conditions there are effectively no damping mechanisms in the nonresonant portion of the chamber, so we must explain these amplitude changes by the nonuniform magnetic field. The amplitudes of E^θ and b^ρ increase as resonance is approached because the wave polarization is changing from elliptical to circular. The amplitude of b^θ is increasing slightly because the phase velocity is decreasing in the decreasing magnetic field. (This is because the wave-energy density $b^2/2\mu_o$ is inversely proportional to phase velocity if there is no damping. However, the wave is spreading radially as it propagates. This competing effect reduces the wave-energy density, so the net increase of b^θ is small.)

The decrease in E^ρ may be understood by replacing ∇ with $i\,k\,\hat{z}$ in the Maxwell equation (2.4) and solving for $\underline{E}$:

$$\underline{E} = \frac{\omega}{k}\,\underline{b} \times \hat{z}.$$

This shows that the amplitude of $\underline{E}$ is proportional to the phase velocity if the amplitude of $\underline{b}$ does not change. Since the phase velocity is decreasing

in the decreasing magnetic field, E^{ρ} is also decreasing.

4. Phase Velocity

The phase velocity is proportional to the spacing between contours in the absence of reflections. In the downstream end of the chamber the phase velocity can be deduced from the half wave length between nodes. The phase velocity conforms to the analytic theory for the torsional mode where the magnetic field is above resonance. Near the midplane where the magnetic field is below resonance, the torsional mode is evanescent with a large phase velocity.

The compressional mode in the electrode images is excited by the j^{θ} currents in the annular current sheets and is not propagating due to the waveguide cutoff. Its apparent phase velocity is therefore primarily determined by the phase of j^{θ} and is almost equal to the phase velocity of the torsional mode.

C. Solutions for Low Densities (1 to $3\times10^{19}\,m^{-3}$)

Figure 7 shows a solution with an assumed density of $3.0\times10^{19}\,m^{-3}$, which is about one-fifth that of the previously discussed density. All other parameters are unchanged. This result is somewhat closer to the experimental wave measurements, and is complicated by larger reflections from the resonance.

The reflections are excited by an interesting mechanism. The transverse current is concentrated in a toroid near the ion-cyclotron resonance. The j^{θ} component excites a fairly large axial rf magnetic field (b^{ζ}) near the j^{θ} toroid. (The j^{θ} and b^{ζ} plots are similar to those of Fig. 5, but are spatially more concentrated.) The energy associated with this b^{ζ} magnetic field cannot be absorbed by ion-cyclotron damping nor can it propagate in the

compressional mode in this low density. This energy is reflected as a wave propagating across magnetic-field lines from the concentrated b^{ζ} source. The result is a diagonal pattern of standing waves most clearly shown by the amplitude of b^{θ}, Fig. 7. This pattern is formed by the interaction of the incident wave propagating axially and the reflected wave propagating in a direction with a large transverse component. It should be noted that this mechanism would not be found by a theory that assumes either an unbounded medium or purely axial propagation.

The effect of reflections upon the phase can be large even when the reflected power is small, as illustrated by this example. By comparing the amplitudes of the nodes and antinodes in this standing-wave pattern, it is found that the amplitude of the reflected wave is about one-half the incident amplitude and that the reflected power is therefore about 25%. Similar solutions have been obtained for lower plasma densities, and it is found that reflections are larger and the results are therefore more complicated in appearance. For densities below $10^{19} m^{-3}$, most of the energy is reflected from the resonance. This is basically because the wavelength of the torsional mode becomes too long relative to the dimensions of the magnetic mirror for efficient ion-cyclotron damping.

The reflection pattern disappears when some other type of damping is introduced. Figure 8 shows the phase and amplitude of b^{θ} for conditions identical to those of Fig. 7, except that a density of neutral particles equal to the ion density has been specified. (Such a pessimistic condition could conceivably arise if the experiment were dominated by charge-transfer collisions.) No reflections occur in this condition because the b^{ζ} wave is damped by neutral damping but not by cyclotron damping. We find that the damping near the resonance is almost entirely caused by neutral particles.

D. Comparison of Experimental and Numerical Results

Experimentally measured wave amplitudes agree well with results of the numerical model provided reflections are not too large. The amplitude of b^{θ} was numerically found to be insensitive to plasma density except for the effect of reflections. The experimental data contain suggestions of small reflections, but the reflected amplitude is at most 20% of the incident amplitude. (This is the extent of amplitude variations in the nonresonant portion of the experiment, which may have masked the standing waves.)

The high-phase velocity (7.5×10^{6} m/sec) deduced from the experimental data[2] implies a substantial reduction of plasma density. The density reduction is probably not entirely responsible for the phase velocity measurement, since the density and temperature measurements by diamagnetic probe and Doppler broadening are inconsistent with densities below $10^{19}m^{-3}$.[13]

Possibly the phase measurements were affected by small (20%) reflections or by density nonuniformities that were not detected experimentally because of shot-to-shot differences. Some numerical solutions have been obtained with radial density gradients that indicate complicated effects on the phase that would have been impossible to measure in detail.

A self-consistent set of parameters that reasonably satisfies the findings of the wave measurements, the numerical results, and the diagnostics is listed below.

Ion density	2×10^{19} m^{-3}
Neutrals and impurities	10%
Ion temperature	50 eV at the resonance, 25 eV elsewhere
Electron temperature	20 eV at the resonance, 10 eV elsewhere

The lack of large reflections at this density could be accounted for by the presence of neutrals and impurities. This set of parameters is not a unique set of values satisfying the results, but is reliable within a factor of about four.

V. CONCLUSIONS

From a combination of the experimental and numerical results, we may conclude that the dominant damping mechanism is ion-cyclotron damping. A small portion of the wave energy may have been reflected, but large reflections would have been experimentally observed. Damping by neutral particles may be ruled out as a dominant mechanism since the energy absorption by neutrals would not have produced the diamagnetic signal. This implies a high ionization maintained by electron temperatures of about 10 eV. For such electron temperatures the ohmic resistivity is several orders of magnitude below the cyclotron resistivity. For the reasons given in reference 13, we must believe the damping by impurity ions to be less than the neutral damping.

The points of agreement between the experiment and the numerical model indicate that the physical principles on which the model is based are generally correct. Some of the assumed conditions do not conform precisely to the experiment; and some of the experimental measurements may have missed some complications found by the numerical model. The model has improved the understanding of the excitation and propagation of the two hydromagnetic modes and of the damping and reflection mechanisms at the ion-cyclotron resonance.

ACKNOWLEDGMENTS

The author wishes to thank Drs. Forrest I. Boley, Wulf B. Kunkel, and John M. Wilcox and Mr. William R. Baker for advice and encouragement during this work. Advice on the matrix iteration technique was provided by Dr. Gene Golub of the Stanford Computation Center, Stanford University. Assistance was furnished by many individuals at the E. O. Lawrence Radiation Laboratory, especially in the Sherwood Physics Group and in the Mathematics and Computing Section of the Theoretical Physics Group.

The author was supported by a National Science Foundation Graduate Fellowship.

FOOTNOTES AND REFERENCES

*Work done under the auspices of the U. S. Atomic Energy Commission.

†Present address: Aerojet General Nucleonics, San Ramon, California

1. W. M. Hooke and M. A. Rothman, A Survey of Experiments on Ion Cyclotron Resonance in Plasma, Nucl. Fusion 4, 33 (1964).
2. F. I. Boley, J. M. Wilcox, A. W. DeSilva, P. R. Forman, G. W. Hamilton, C. N. Watson-Munro, Hydromagnetic Wave Propagation near Ion Cyclotron Resonance, Phys. Fluids 6, 925 (1963).
3. T. H. Stix, The Theory of Plasma Waves, (McGraw-Hill Book Co., N. Y., 1962).
4. W. P. Allis, S. J. Buchsbaum, and A. Bers, Waves in Anisotropic Plasmas, (M. I. T. Press, Cambridge, Massachusetts, 1963).
5. Alan W. DeSilva, Experimental Study of Hydromagnetic Waves in Plasma (Ph. D. Thesis), Lawrence Radiation Laboratory Report UCRL-9601, March 1961 (unpublished).
6. David Larry Sachs, The Effect of Collisions on Ion Cyclotron Waves (Ph. D. Thesis), Lawrence Radiation Laboratory Report UCRL-11407, May 1964 (unpublished).
7. A. G. Engelhardt and A. A. Dougal, Dispersion of Ion Cyclotron Waves in Magnetoplasmas, Phys. Fluids 5, 29 (1962).
8. K. N. Stepanov, Propagation of Ion Cyclotron Plasma Waves in a Weakly Inhomogeneous Field, Nucl. Fusion 3, 154 (1963).
9. C. S. Roberts and S. J. Buchsbaum, Motion of a Charged Particle in a Constant Magnetic Field and a Transverse Electromagnetic Wave Propagating along the Field, Phys. Rev. 135, A384 (1964).

10. A. Legatowicz, Heating of Plasma in a Circularly Polarized Electromagnetic Wave, Nucl. Fusion 3, 1 (1963).

11. A. Hakkenberg and M. P. H. Weenink, The Motion of a Charged Particle in a Constant Homogeneous Magnetic Field and an Electromagnetic Wave Propagating Parallel to the Magnetic Field, Rijhuizen Report 64-18 (Associate Euratom-Fom Institut Voor Plasma-Fysica, Rijnhuizen-Jutphaas-Nederland, 1963).

12. L. Spitzer, Jr., Physics of Fully Ionized Gases, 2nd revised edition, (Interscience Publishers, New York, 1962).

13. G. W. Hamilton, Absorption of Ion Cyclotron Waves (Ph. D. Thesis), Lawrence Radiation Laboratory Report UCRL-11619, September 1964 (unpublished).

14. R. S. Varga, Matrix Iterative Analysis, (Prentice-Hall, Inc., Englewood Cliffs, N. J., 1962).

15. D. G. Swanson, R. W. Gould, and R. H. Hertel, Phys. Fluids 7, 269 (1964).

16. George R. Spillman, A Study of Hydromagnetic Wave Propagation in Plasma (Ph. D. Thesis), Lawrence Radiation Laboratory Report UCRL-10990, October 1963 (unpublished).

FIGURE LEGENDS

Fig. 1. Nonorthogonal coordinate system. The transverse coordinate lines are orthogonal to magnetic flux lines, whereas the axial coordinate lines are parallel to the centerline.

Fig. 2. Nonorthogonal mesh system.

Fig. 3. Experimental apparatus.

Fig. 4. B^z and B^r as functions of position, for the standard mirror field. The three curves on each graph indicate the magnetic fields at three radii: 0.76 cm, 5.3 cm, and 9.9 cm.

Fig. 5. Solution of MHD wave equations for conditions of Sec. IV.B. Wave currents and axial-wave magnetic field are shown.

Fig. 6. Solution of MHD wave equations for conditions of Sec. IV.B. Amplitudes and phases of transverse-wave magnetic fields are shown.

Fig. 7. Solution of MHD wave equations for conditions of Sec. IV.C. Amplitude and phase of azimuthal wave magnetic field are shown.

Fig. 8. Solution of MHD wave equations with neutral damping. Amplitude and phase of azimuthal-wave magnetic field are shown.

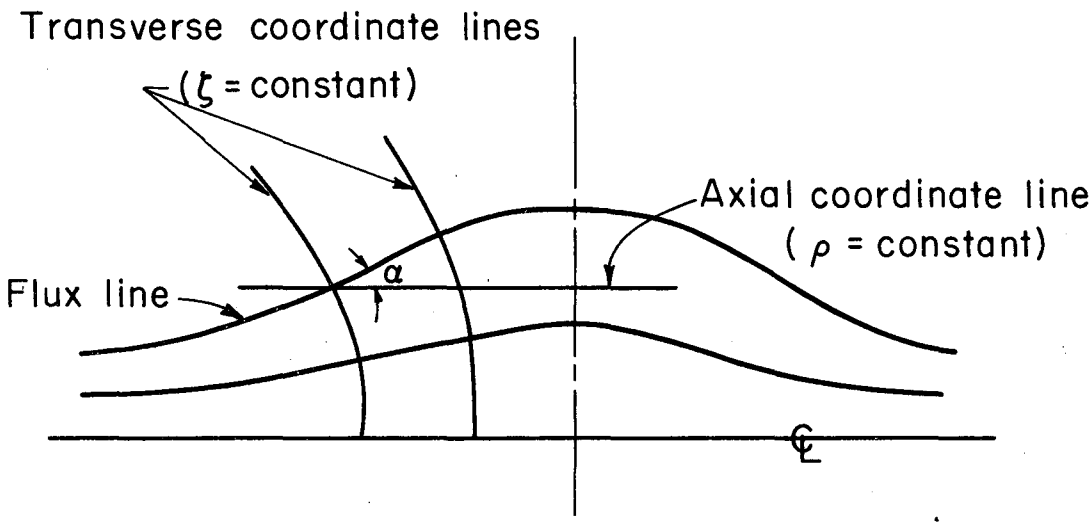

MU-34715

Fig. 1

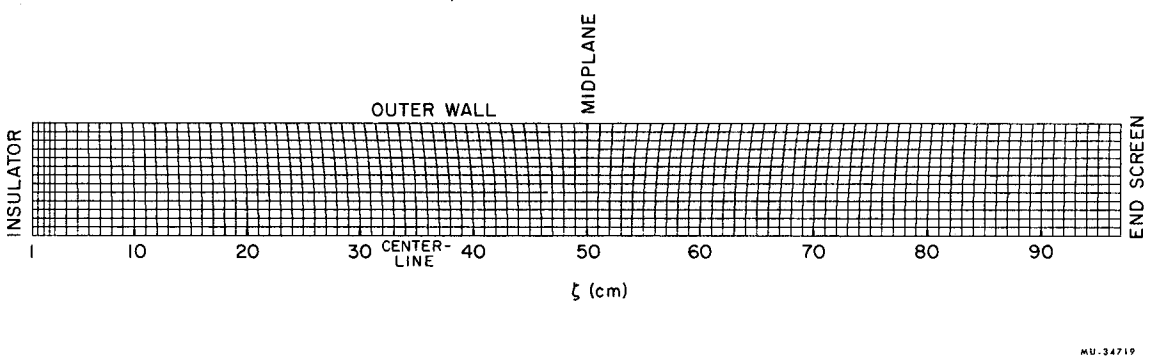
MIDPLANE
OUTER WALL
INSULATOR
END SCREEN
1
10
20
30
CENTER-LINE
40
50
60
70
80
90
ζ (cm)
MU-34719

Fig. 2

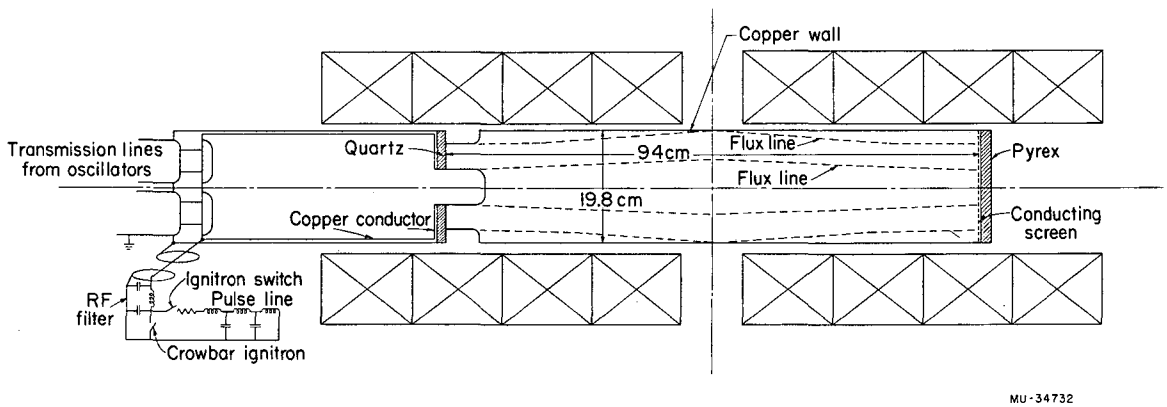
Copper wall
Transmission lines
from oscillators
Quartz
94cm
Flux line
Flux line
Pyrex
19.8 cm
Copper conductor
Conducting
screen
Ignitron switch
Pulse line
RF
filter
Crowbar ignitron
MU-34732

Fig. 3

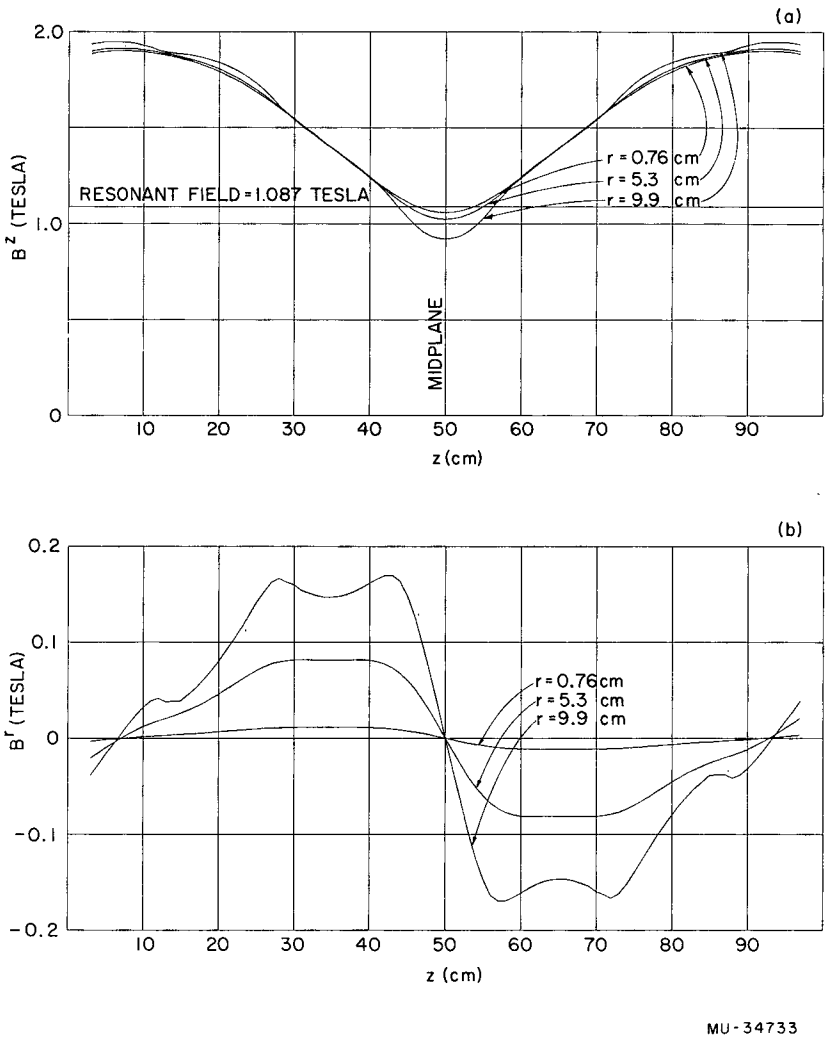
(a)
2.0
1.0
0
B^z (TESLA)
RESONANT FIELD = 1.087 TESLA
r = 0.76 cm
r = 5.3 cm
r = 9.9 cm
MIDPLANE
10
20
30
40
50
60
70
80
90
z (cm)
(b)
0.2
0.1
0
-0.1
-0.2
B^r (TESLA)
r = 0.76 cm
r = 5.3 cm
r = 9.9 cm
10
20
30
40
50
60
70
80
90
z (cm)
MU-34733

Fig. 4

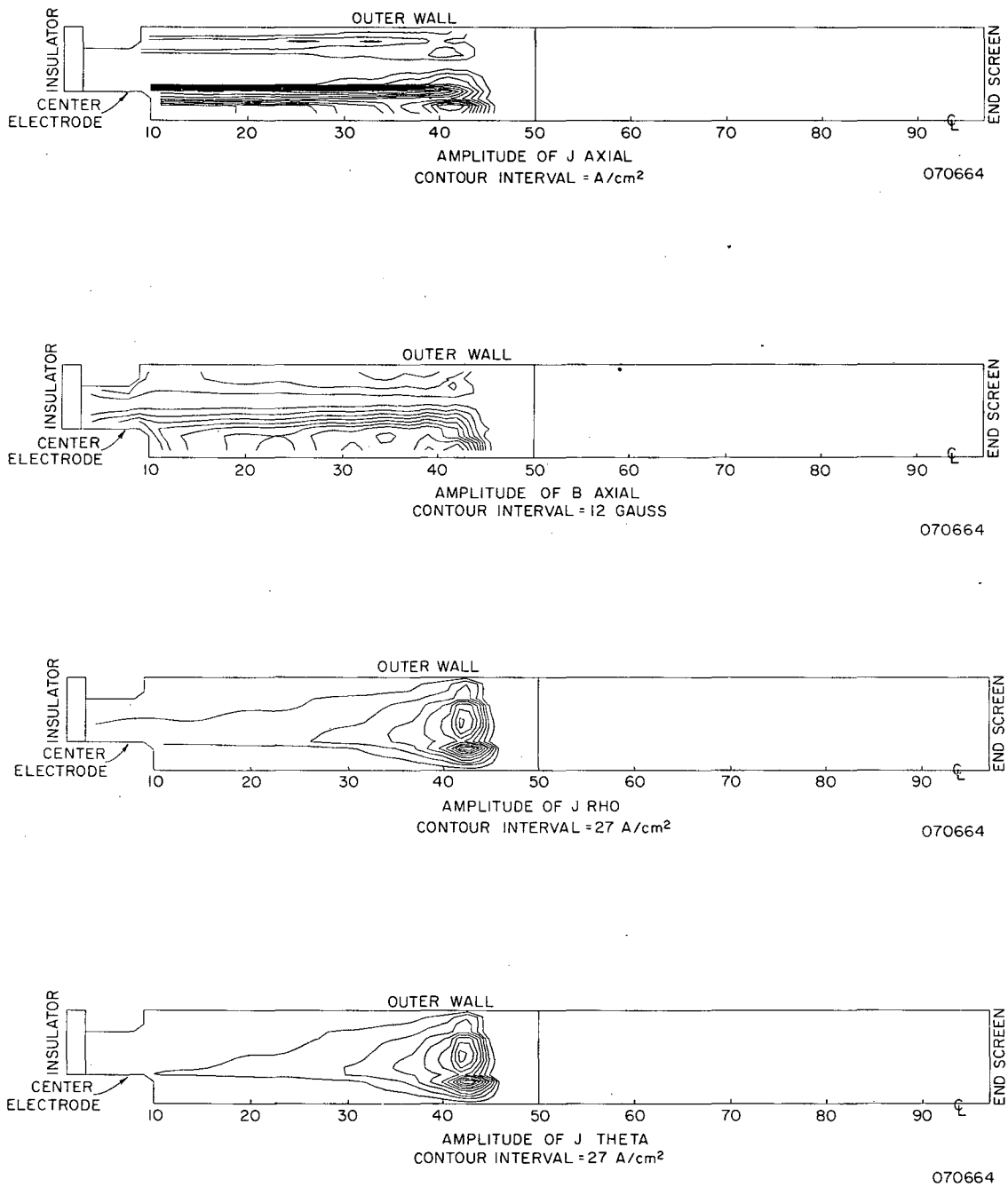

MUB-4976

Fig. 5

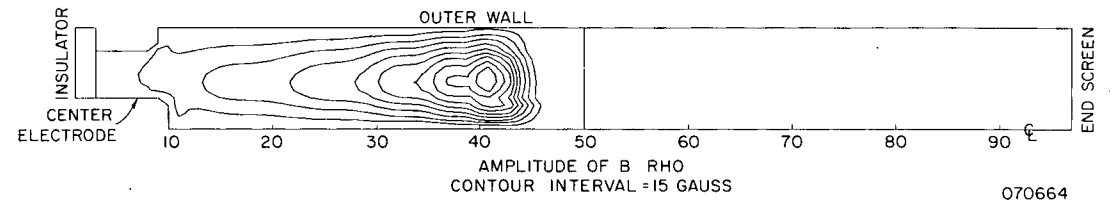

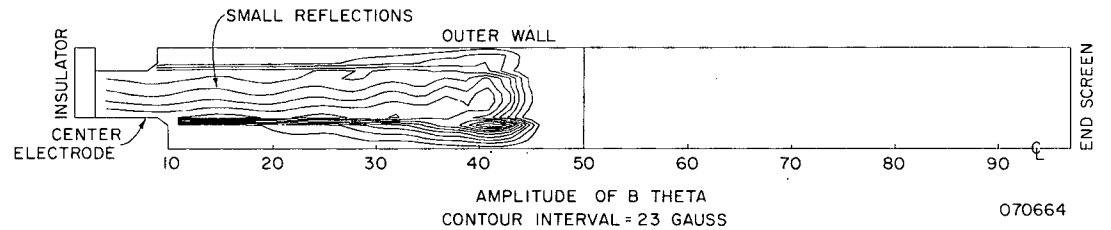

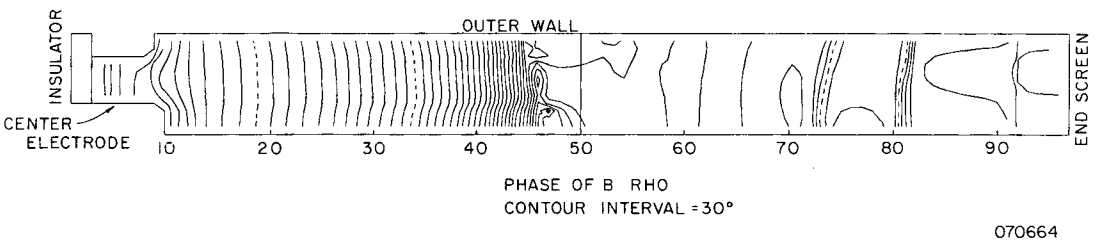

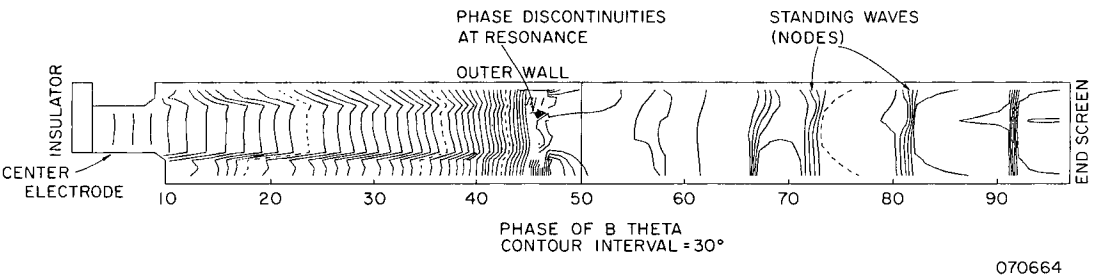

MUB-4977

Fig. 6

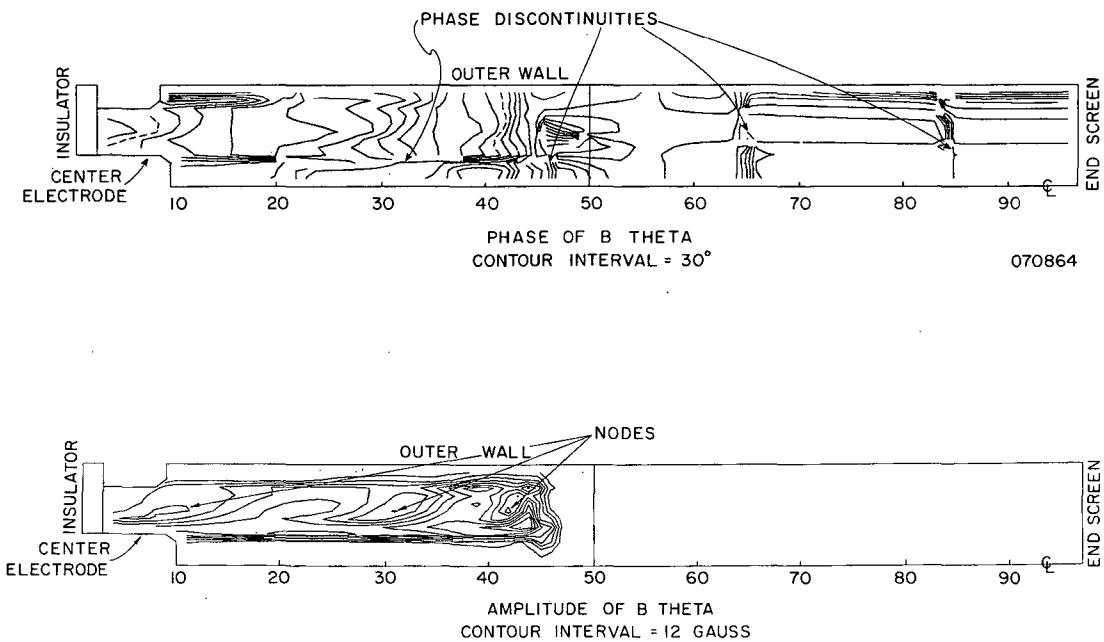

MUB-4978

Fig. 7

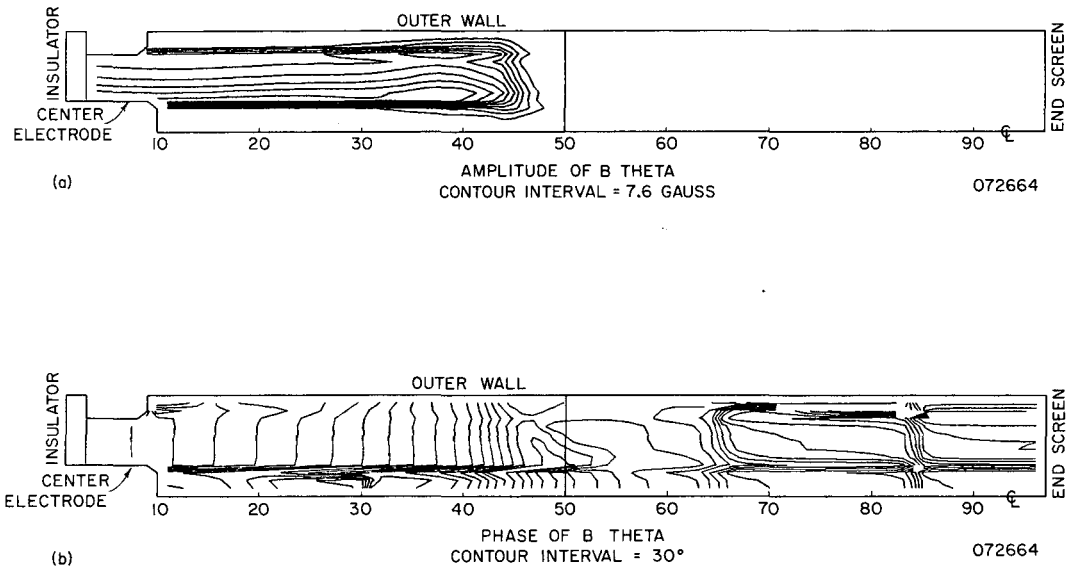
OUTER WALL
INSULATOR
CENTER ELECTRODE
END SCREEN
10
20
30
40
50
60
70
80
90
(a)
AMPLITUDE OF B THETA
CONTOUR INTERVAL = 7.6 GAUSS
072664
OUTER WALL
INSULATOR
CENTER ELECTRODE
END SCREEN
10
20
30
40
50
60
70
80
90
(b)
PHASE OF B THETA
CONTOUR INTERVAL = 30°
072664
MU-34731

Fig. 8

This report was prepared as an account of Government sponsored work. Neither the United States, nor the Commission, nor any person acting on behalf of the Commission:

A. Makes any warranty or representation, expressed or implied, with respect to the accuracy, completeness, or usefulness of the information contained in this report, or that the use of any information, apparatus, method, or process disclosed in this report may not infringe privately owned rights; or

B. Assumes any liabilities with respect to the use of, or for damages resulting from the use of any information, apparatus, method, or process disclosed in this report.

As used in the above, "person acting on behalf of the Commission" includes any employee or contractor of the Commission, or employee of such contractor, to the extent that such employee or contractor of the Commission, or employee of such contractor prepares, disseminates, or provides access to, any information pursuant to his employment or contract with the Commission, or his employment with such contractor.